




# $^{119}\text{Sn}$ Mössbauer spectroscopy for assessing the local stress and defect state towards the tuning of Ni-Mn-Sn alloys

Cite as: Appl. Phys. Lett. **110**, 181908 (2017); <https://doi.org/10.1063/1.4982630>

Submitted: 16 March 2017 . Accepted: 12 April 2017 . Published Online: 02 May 2017

I. Unzueta, J. López-García, V. Sánchez-Alarcos, V. Recarte , J. I. Pérez-Landazábal , J. A. Rodríguez-Velamazán , J. S. Garitaonandia, J. A. García, and F. Plazaola



View Online



Export Citation



CrossMark

## ARTICLES YOU MAY BE INTERESTED IN

**Magnetic and martensitic transformations of NiMnX (X = In, Sn, Sb) ferromagnetic shape memory alloys**

Applied Physics Letters **85**, 4358 (2004); <https://doi.org/10.1063/1.1808879>

**Mössbauer study on martensite phase in  $\text{Ni}_{50}\text{Mn}_{36.5}^{57}\text{Fe}_{0.5}\text{Sn}_{13}$  metamagnetic shape memory alloy**

Applied Physics Letters **93**, 042509 (2008); <https://doi.org/10.1063/1.2960551>

**Large magnetic-field-induced strains in  $\text{Ni}_2\text{MnGa}$  single crystals**

Applied Physics Letters **69**, 1966 (1996); <https://doi.org/10.1063/1.117637>

This article may be downloaded for personal use only. Any other use requires prior permission of the author and AIP Publishing.

Lock-in Amplifiers  
up to 600 MHz



# **$^{119}\text{Sn}$ Mössbauer spectroscopy for assessing the local stress and defect state towards the tuning of Ni-Mn-Sn alloys**

I. Unzueta,<sup>1,2,a)</sup> J. López-García,<sup>3,4</sup> V. Sánchez-Alarcos,<sup>4,5</sup> V. Recarte,<sup>4,5</sup>  
 J. I. Pérez-Landazábal,<sup>4,5</sup> J. A. Rodríguez-Velamazán,<sup>3</sup> J. S. Garitaonandia,<sup>6,2</sup>  
 J. A. García,<sup>6,2</sup> and F. Plazaola<sup>1</sup>

<sup>1</sup>Department of Electricity and Electronics, University of the Basque Country UPV/EHU, 48940 Leioa, Spain

<sup>2</sup>BCMaterials, University of the Basque Country UPV/EHU, 48940 Leioa, Spain

<sup>3</sup>Institut Laue-Langevin, 71 Avenue des Martyrs, 38000 Grenoble, France

<sup>4</sup>Department of Physics, Universidad Pública de Navarra, Campus de Arrosadía, 31006 Pamplona, Spain

<sup>5</sup>Institute for Advanced Materials (INAMAT), Universidad Pública de Navarra, Campus de Arrosadía, 31006 Pamplona, Spain

<sup>6</sup>Department of Applied Physics II, University of the Basque Country UPV/EHU, 48940 Leioa, Spain

(Received 16 March 2017; accepted 12 April 2017; published online 2 May 2017)

The influence of defects and local stresses on the magnetic properties and martensitic transformation in  $\text{Ni}_{50}\text{Mn}_{35}\text{Sn}_{15}$  is studied at macroscopic and atomic scale levels. We show that both the structural and magnetic properties of the alloy are very sensitive to slight microstructural distortions. Even though no atomic disorder is induced by milling, the antiphase boundaries linked to dislocations promote the antiferromagnetic coupling of Mn, resulting in a significant decrease in the saturation magnetization. On the other hand, the temperature range of the transformation is considerably affected by the mechanically induced local stresses, which in turn does not affect the equilibrium temperature between the austenitic and martensitic phases. Finally, we demonstrate that the recovery of the martensitic transformation is directly related to the intensity of the non-magnetic component revealed by  $^{119}\text{Sn}$  Mössbauer spectroscopy. This result opens the possibility of quantifying the whole contribution of defects and the local stresses on the martensitic transformation in Ni-Mn-Sn alloys.

Published by AIP Publishing. [<http://dx.doi.org/10.1063/1.4982630>]

Ni-Mn based Heusler alloys have been extensively studied during the last two decades due to the multifunctional properties they exhibit such as large magnetic-field-induced strain,<sup>1,2</sup> magnetoresistivity,<sup>3,4</sup> magnetocaloric effects,<sup>5–8</sup> exchange bias,<sup>9,10</sup> and shape-memory effects.<sup>11</sup> These properties are linked to the occurrence of a martensitic transformation (MT) between magnetically ordered phases. In the case of metamagnetic shape memory alloys  $\text{Ni}_2\text{Mn-Z}$  ( $Z = \text{In}, \text{Sn}, \text{and Sb}$ ), the MT occurs between ferromagnetic austenite and weak magnetic martensite, thus giving rise to interesting properties such as magnetic-field induced shape memory effects<sup>12–15</sup> and inverse magnetocaloric effects.<sup>16–18</sup>

Despite the promising features, these alloys have very poor mechanical properties, and their brittleness and fragility hinder the development of practical devices. In order to overcome the limitations of the bulk material, several alternatives have been investigated, such as the use of alloys in the form of ribbons,<sup>19</sup> foams,<sup>20</sup> or films,<sup>21</sup> as well as embedding shape memory particles in a polymer matrix.<sup>22,23</sup> As a result, the use of microparticles as microactuator elements is attracting an increasing interest during the last few years.<sup>24–27</sup>

In order to enhance the multifunctional properties of the micro-particles and films, the control of defects and the local stress-state becomes fundamental as they influence directly the MT.<sup>28–31</sup> The presence of residual stress increases the thermal hysteresis and the irreversibility of the MT.<sup>32</sup> Residual stress is also retained when the samples are cycled through the phase transformation,<sup>33</sup> being one of the main causes of the

degradation of the MT, the deformation behavior, and the shape memory effect.<sup>34</sup> Additionally, the presence of defects induced during the synthesis of nanoparticles may inhibit the MT<sup>35</sup> and influence the ferromagnetic (FM) interactions.<sup>36</sup> Thus, the characterization of defects, the local stress-state, and their influence on the MT will provide a more proper tuning of the structural and magnetic properties of these alloys for more extensive applications.<sup>27,37</sup> In particular, Ni-Mn-Sn alloys have been extensively studied because of their enhanced magnetocaloric properties<sup>38</sup> and the high stability of their long-range atomic order structure against thermal treatments.<sup>39</sup>

Mössbauer spectroscopy (MS) is a powerful technique for both structural and magnetic characterization at the atomic level. Although several works can be found, in which  $^{57}\text{Fe}$  MS has been used in Fe doped Ni-Mn-Sn alloys,<sup>36,40–42</sup>  $^{119}\text{Sn}$  MS, which makes doping unnecessary and therefore helps to ensure chemical environment of Sn atoms, has been scarcely employed.<sup>43</sup> In fact, the present work demonstrates that even though no atomic disorder is induced, defects and local stresses greatly affect the MT, which can be directly quantified by  $^{119}\text{Sn}$  MS. The obtained results are especially interesting as long as the modification of defects configuration could be, along with composition, the only way to properly tune the functional properties in these systems.

A polycrystalline ingot of  $\text{Ni}_{50}\text{Mn}_{35}\text{Sn}_{15}$  was synthesized from high purity elements by arc melting under the protective argon atmosphere. The obtained alloy was homogenized at 1173 K for 24 h, and its composition was checked by EDX analysis. With the aim of inducing defects, the alloy

<sup>a)</sup>Electronic mail: iraultza.unzueta@ehu.eus

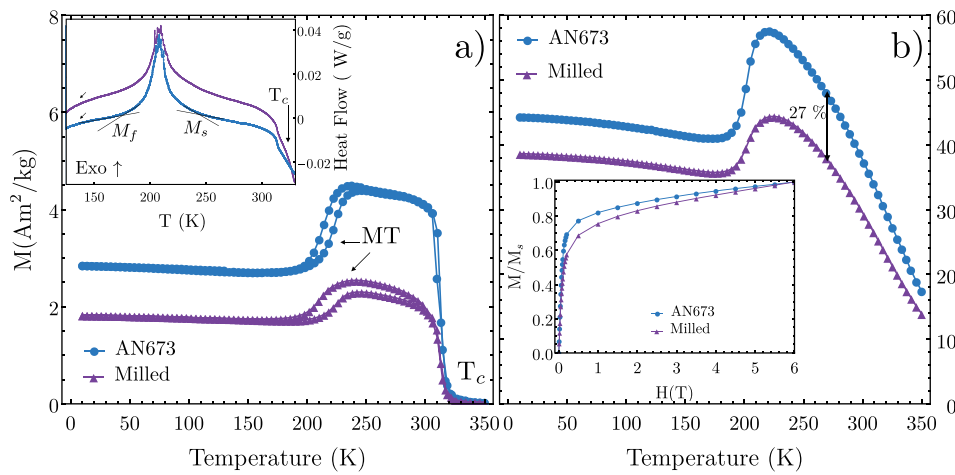


FIG. 1.  $M(T)$  for the Milled and AN673 samples recorded at 0.01 T (a) and 6 T (b). The inset in (a) shows the DSC of both samples. The inset in (b) shows the normalized  $M(H)$  cycle of both Milled and AN673 samples recorded at 270 K.

was mechanically milled in an agate mortar until reaching a steady state in the spectra revealed by  $^{119}\text{Sn}$  MS. Then, in order to analyze the microstructural evolution upon post-milling, several milled powder samples were taken and separately annealed at 573, 673, 773, and 873 K for 5 min at each temperature (labeled as Milled, AN573, AN673, AN773, and AN873, respectively). Calorimetric measurements were carried out in a TA Q100 DSC at a heating/cooling rate of 10 K/min, and the magnetic characterization was performed using a QD MPMS XL-7 SQUID magnetometer. Powder neutron diffraction (PND) measurements were performed using a D2B instrument ( $\lambda = 1.59$  Å) at the Institute Laue-Langevin in Grenoble (France [Institute Laue-Langevin in Grenoble, France (J. López-García, J. I. Pérez-Landazábal, V. Recarte, J. A. Rodríguez-Velamazán, V. Sánchez-Alarcos, I. Unzueta, DOI:10.5291/ILL-DATA.5-24-591]). The FullProf<sup>44</sup> program was employed for the Rietveld refinement. Mössbauer spectra were obtained using a  $\text{Ba}^{119}\text{SnO}_3$  source in a transmission setup at 270 K and fitted using NORMOS program.

Fig. 1 shows the temperature dependence of magnetization at 0.01 T (1(a)) and 6 T (1(b)) for both the Milled and the AN673 samples. As shown in Fig. 1(a), annealing does not affect neither the  $T_c$  nor the MT temperature (the same behaviour is observed for the rest of the AN573, AN773, and AN873 samples, not shown here). This can be also inferred from the DSC measurements (see the inset of Fig. 1(a)), which, in turn, show a narrower temperature range of the MT for the AN673 sample, indicating a decrease in the elastic energy term as a result of annealing.<sup>29</sup> Taking into account that both  $T_c$  and the MT temperature are highly

sensitive to atomic order,<sup>45</sup> the lack of variation in these transition temperatures seems to indicate a null effect of annealing in the atomic order.<sup>39</sup> Nevertheless, as shown in Fig. 1(b), the high-field magnetization increases in both austenite and martensite on annealing. Furthermore, the different approach to saturation shown in the normalized  $M(H)$  curves measured at 270 K (inset Fig. 1(b)) points out a different antiferromagnetic (AF) contribution to the magnetic moment between the Milled and AN673 samples.

The crystallographic structure and long-range atomic order of the studied samples have been analyzed from PND measurements. Figs. 2(a) and 2(b) show the experimental and fitted diffractograms obtained from the Milled and AN673 samples at 270 K (ferromagnetic austenite). Both samples show the cubic  $L2_1$  ( $\text{Fm}\bar{3}\text{m}$ ) structure with the same lattice parameter (6.004(1) Å for the Milled sample and 6.003(1) Å for the AN673 sample). The magnetic and structural parameters for 4(a) and 4(b) positions obtained after Rietveld refinement are shown in Table I. The occupancies are almost the same in both cases (4(a) positions are mainly occupied by Mn atoms and 4b positions are occupied by both Mn and Sn atoms,<sup>46</sup> as illustrated in Fig. 2(c)), which means that the degree of  $L2_1$  atomic order is the same in both samples. Therefore, in agreement with the observed absence of variation in the transition temperatures, no atomic order variation is brought by annealing. Nevertheless, interestingly, the magnetic coupling between Mn atoms in 4a and 4b positions drastically evolves from AF to FM upon annealing, in spite of neither atomic order nor lattice parameter does. Such evolution is indeed in line with the observed increase in the

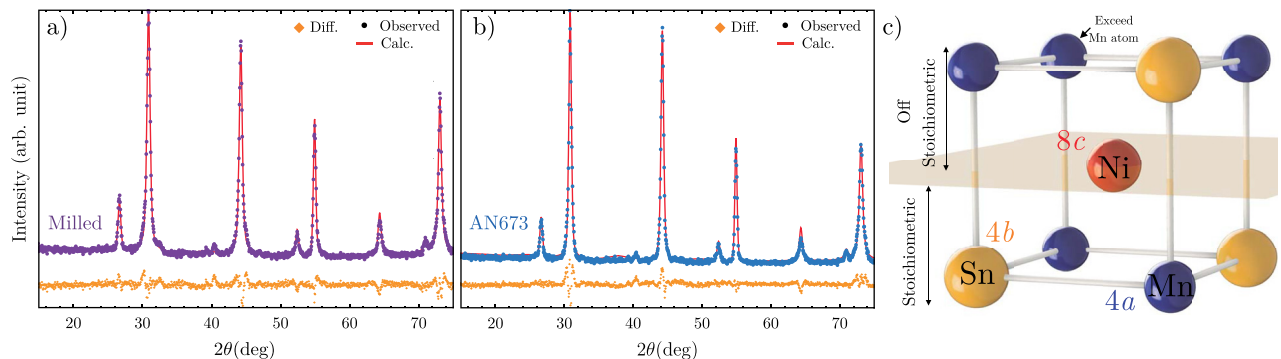


FIG. 2. Rietveld refinement of the diffraction patterns for the Milled (a) and AN673 samples (b) recorded at 270 K. (c) Preferred positions of Mn and Sn atoms in stoichiometric and off-stoichiometric conditions.

TABLE I. Occupancies and magnetic moment values ( $\mu$ ) for 4a, 4b, and 8c positions obtained from the Rietveld refinement for the Milled and AN673 samples. For 8c position,  $\mu = 0$  is considered.

	Site 4a		Site 4b		Site 8c
	Occupancy	$\mu(\mu_B)$	Occupancy	$\mu(\mu_B)$	Occupancy
Milled	Mn 0.95(4)		Mn 0.41(4)		Mn 0.08(1)
	Ni 0.05(4)	1.26(6)	Ni 0.02(0)	-0.45(6)	Ni 0.92(1)
	Sn (—)		Sn 0.57(4)		Sn (—)
AN673	Mn 0.94(3)		Mn 0.43(3)		Mn (—)
	Ni 0.06(3)	2.58(2)	Ni 0.05(0)	0.37(2)	Ni 1(-)
	Sn (—)		Sn 0.52(3)		Sn (—)

high-field magnetization. In this respect, it is worth noting that the reflection peaks are clearly broader in the Milled sample. This points out a microstructural evolution (higher crystallite size or lower microstrains in the annealed sample), which could be behind the magnetic one.

In order to ascertain the nature of the effect of annealing on the magnetic properties, the magnetism has been studied at the atomic level by  $^{119}\text{Sn}$  MS. Fig. 3 shows the experimental and fitted  $^{119}\text{Sn}$  Mössbauer spectra of all the samples. The spectrum of the Milled sample is mainly composed of a non-magnetic singlet with a non-resolved magnetic component as a minor contribution. The relative intensity of both

components changes gradually with the annealing temperature, being the magnetic subspectrum practically the only contribution to the spectrum of the AN873 sample. All the spectra have been satisfactorily fitted exclusively with these two discrete contributions.

The values obtained from the fitting of Mössbauer spectra are listed in Table II. The main common feature is the decrease in the singlet component ( $A_s$ ) and increase in the  $B_{hf}$  magnetic hyperfine field, with increasing annealing temperature. Similar values of the  $\delta$  isomer shift of both components have been obtained for all the samples, indicating that the chemical order in the surrounding of Sn atoms remains the same, independently of the annealing process.<sup>47</sup> However, the line-width parameter  $\Gamma$  listed in Table II decreases as the annealing temperature increases. The  $\Gamma$  parameter is sensitive to the slight distortions of the local environment of the Mössbauer probe atoms,<sup>48</sup> so its decrease indicates a microstructural recovery on the very close environment of Sn atoms.

In a nutshell, PND, MS, and magnetic measurements point out the lack of atomic disorder differences between the studied samples. However, the decrease of the  $\Gamma$  parameter and the narrowing of the PND peaks with the increasing annealing temperature suggest an evolution in the microstructural parameters. Thereby, the observed changes in the magnetic properties and in the width of the MT would rely

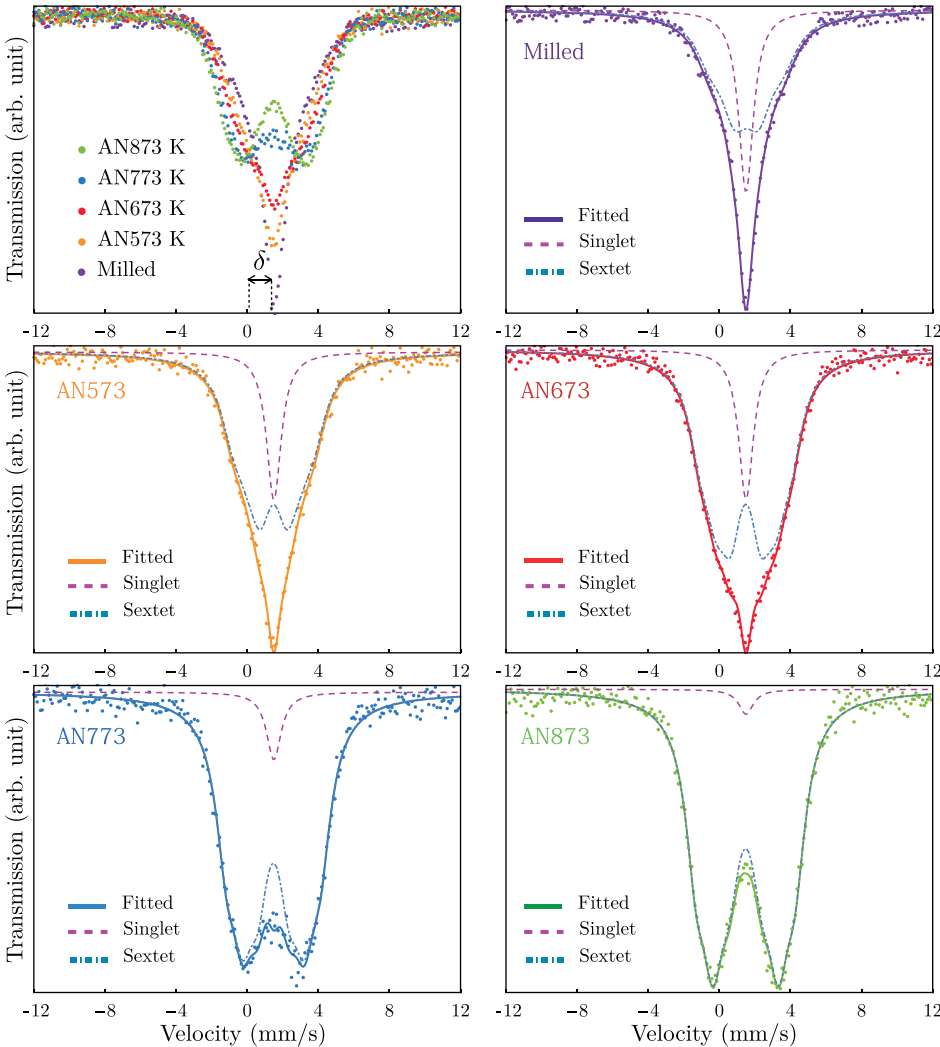


FIG. 3. Raw (up left) and fitted Mössbauer spectra of the Milled and all annealed samples at 270 K.



TABLE II.  $\delta$  isomer shift,  $\Gamma$  line-width, the hyperfine field  $B_{hf}$ , and the area of the singlet component  $A_s$  obtained from the fitting procedure of the Mössbauer spectra for all the studied samples.

Sample	$\delta$ (mm/s) <sup>a</sup>	$\Gamma$ (mm/s) <sup>a</sup>	$B_{hf}$ (T)	$A_s$ (%)
Milled	1.53(1)	1.96(1)	4.1(1)	%31(3)
AN573	1.48(1)	1.67(7)	4.6(2)	%18(1)
AN673	1.48(1)	1.54(5)	5.2(1)	%15(1)
AN773	1.48(1)	1.51(4)	5.3(1)	%6(1)
AN873	1.48(1)	1.50(2)	5.6(1)	%1(1)

<sup>a</sup>Constrained to be the same for both subspectra.

on different internal stress states and the presence of defects created during the milling.

As previously reported in some Heusler alloys, several local distortions as dislocations and defects can be created during mechanical treatments (i.e., cold working) without inducing any atomic disorder.<sup>49,50</sup> Specifically, the presence of superlattice dislocations in cold worked Heusler alloys is accompanied by anti-phase boundaries (APB).<sup>51,52</sup> Besides, the exchange interaction between the second nearest neighbor (SNN) Mn atoms located across the APB can become AF in an otherwise FM material.<sup>53,54</sup>

Although the SNN of Mn is Sn atoms at  $4b$  positions, in off-stoichiometric conditions, the excess Mn occupy  $4b$  positions (see Fig. 2(c)). As listed in Table I, the coupling of  $4a$  and  $4b$  positions is mostly AF in the Milled sample. However, when the samples are annealed, the FM coupling is recovered. Taking into account that the number of AF coupled Mn atoms is proportional to the dislocation density,<sup>51</sup> the annihilation of dislocations results in a decrease in the density of the APB present in the sample, in such a way that the number of AF coupled Mn atoms decreases and the FM coupling is reinforced. Hence, the magnetization is greater in the AN673 sample than in the Milled sample. Additionally, as shown in Fig. 1(b), the magnetization of the AN673 sample approaches better saturation than the Milled sample.

The annihilation of dislocations also explains the reduction of the  $\Gamma$  parameter and the narrowing of PND peaks after the annealing.<sup>54</sup> The release of the local stress associated with dislocations homogenizes the surrounding environment of Sn atoms and, as a consequence, the value of  $\Gamma$  decreases. As shown in Table II, the major recovery of  $\Gamma$  occurs in the first two annealing at 573 K and 673 K. The annihilation of the dislocations at these temperatures has been previously reported in other Heusler alloys.<sup>49,52</sup> However, as the  $^{119}\text{Sn}$  MS shows in Fig. 3, the recovery process continues above 673 K without a significant change in  $\Gamma$ . In this region, the recovery would be mediated by the elimination of point defects such as vacancies.<sup>55</sup>

Sn atoms do not carry intrinsic magnetic moment, but a transferred hyperfine field can be induced from the neighboring magnetic ions (Mn ions in the case of Ni-Mn-Sn).<sup>56</sup>  $^{119}\text{Sn}$  Mössbauer spectra would reflect the local magnetic field felt by the Sn atoms. The singlet component observed by MS (Fig. 3), related to stressed regions caused by dislocations and APB, indicates the absence of the local magnetic field. Thus, this component points out that the ferromagnetic order is altered in the region of influence of the APB in such

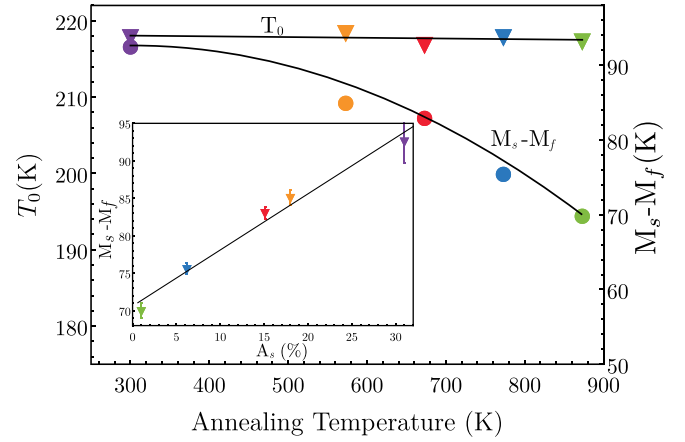


FIG. 4. Evolution of the  $T_0$  parameter (triangles) and the  $M_s - M_f$  (full dots) as a function of the annealing temperature. The inset shows the mutual dependence between the  $M_s - M_f$  parameter and  $A_s$ .

a way that the total transferred dipolar field at Sn sites is zero.  $A_s$  decreases as soon as the density of dislocations and APB decreases with annealing at higher temperatures. On the contrary, the  $B_{hf}$  at  $4b$  positions increases (see Table I). In fact,  $B_{hf}$  is  $\approx 27\%$  higher in AN673 than that in the Milled sample, which is exactly the same difference observed in  $M(T)$  of Fig. 1(a) at 270 K. The increase in  $B_{hf}$  implies a reinforcement of the local magnetic field related to the annealing of defects and the recovery of the FM coupling.

With respect to the MT, it is noteworthy that the recovery of the atomic scale magnetism and the annihilation of dislocations and defects do not affect the equilibrium temperature between the austenitic and martensitic phases,  $T_0$ . As shown in Fig. 4,  $T_0$  remains constant irrespective of the annealing temperature.  $T_0$  is highly sensitive to the atomic order,<sup>57</sup> and its constant value reiterates the lack of differences in atomic disorder throughout the studied samples. However, the temperature range in which the MT is extended ( $M_s - M_f$ ) decreases from 92.5 K down to 70 K between the Milled and AN873 samples (see Fig. 4).

As the annealing temperature increases, the non-magnetic regions close to the dislocations decrease, and the intensity of the non-magnetic component revealed by MS decreases. The MS singlet is then directly related to the internal stress-state and the distorted regions that ultimately affect the MT. Therefore, the influence of the microstructural recovery on the MT can be directly tracked by the singlet component revealed by  $^{119}\text{Sn}$  MS. In this respect, the inset in Fig. 4 shows the direct relationship between the intensity of the MS singlet and the width of the temperature range of the MT. As soon as the non-magnetic regions decrease due to the annealing, the  $M_s - M_f$  does behave in the same way.

In conclusion, we show that both MT and magnetic properties of  $\text{Ni}_{50}\text{Mn}_{35}\text{Sn}_{15}$  are very sensitive to slight microstructural distortions even without inducing any change in atomic disorder. Due to the high stability that Ni-Mn-Sn systems show against the atomic disorder, this result opens an additional way to properly tune the functional properties in these systems. Finally, we show that  $^{119}\text{Sn}$  MS can be used to link the MT with the microstructural state, becoming a practical tool to assess the microstructural characterization of the local

stress and defect state in order to properly tune the MT towards future applications.

This work was supported for the Basque Government Grant No. IT-1005-16 by the Spanish Ministry of Economy and Competitiveness under the project MAT2015-65165-C2-R (MINECO/FEDER) and GIC1585. I. Unzueta also wants to acknowledge the Basque Government Grant No. PRE-2014-1-214. ILL and SpINS are acknowledged for beam time allocation. J. López-García acknowledges ILL for his Ph.D. contract.

- <sup>1</sup>K. Ullakko, J. K. Huang, C. Kantner, R. C. O'Handley, and V. V. Kokorin, *Appl. Phys. Lett.* **69**, 1966 (1996).
- <sup>2</sup>M. Chmielus, X. X. Zhang, C. Witherspoon, D. C. Dunand, and P. Mullner, *Nat. Mater.* **8**, 863 (2009).
- <sup>3</sup>S. Y. Yu, Z. H. Liu, G. D. Liu, J. L. Chen, Z. X. Cao, G. H. Wu, B. Zhang, and X. X. Zhang, *Appl. Phys. Lett.* **89**, 162503 (2006).
- <sup>4</sup>W. Ito, K. Ito, R. Y. Umetsu, R. Kainuma, K. Koyama, K. Watanabe, A. Fujita, K. Oikawa, K. Ishida, and T. Kanomata, *Appl. Phys. Lett.* **92**, 021908 (2008).
- <sup>5</sup>A. Planes, L. Mañosa, and M. Acet, *J. Phys. Condens. Matter* **21**, 233201 (2009).
- <sup>6</sup>L. Mañosa, D. González-Alonso, A. Planes, E. Bonnot, M. Barrio, J.-L. Tamarit, S. Aksoy, and M. Acet, *Nat. Mater.* **9**, 478 (2010).
- <sup>7</sup>Z. D. Han, D. H. Wang, C. L. Zhang, H. C. Xuan, B. X. Gu, and Y. W. Du, *Appl. Phys. Lett.* **90**, 042507 (2007).
- <sup>8</sup>T. Krenke, E. Duman, M. Acet, E. F. Wassermann, X. Moya, L. Manosa, and A. Planes, *Nat. Mater.* **4**, 450 (2005).
- <sup>9</sup>M. Khan, I. Dubenko, S. Stadler, and N. Ali, *Appl. Phys. Lett.* **91**, 072510 (2007).
- <sup>10</sup>Y. B. Yang, X. B. Ma, X. G. Chen, J. Z. Wei, R. Wu, J. Z. Han, H. L. Du, C. S. Wang, S. Q. Liu, Y. C. Yang, Y. Zhang, and J. B. Yang, *J. Appl. Phys.* **111**, 07A916 (2012).
- <sup>11</sup>Y. Sutou, Y. Imano, N. Koeda, T. Omori, R. Kainuma, K. Ishida, and K. Oikawa, *Appl. Phys. Lett.* **85**, 4358 (2004).
- <sup>12</sup>K. Oikawa, W. Ito, Y. Imano, Y. Sutou, R. Kainuma, K. Ishida, S. Okamoto, O. Kitakami, and T. Kanomata, *Appl. Phys. Lett.* **88**, 122507 (2006).
- <sup>13</sup>R. Kainuma, Y. Imano, W. Ito, Y. Sutou, H. Morito, S. Okamoto, O. Kitakami, K. Oikawa, A. Fujita, T. Kanomata, and K. Ishida, *Nature* **439**, 957 (2006).
- <sup>14</sup>R. Kainuma, Y. Imano, W. Ito, H. Morito, Y. Sutou, K. Oikawa, A. Fujita, K. Ishida, S. Okamoto, O. Kitakami, and T. Kanomata, *Appl. Phys. Lett.* **88**, 192513 (2006).
- <sup>15</sup>T. Krenke, M. Acet, E. F. Wassermann, X. Moya, L. Mañosa, and A. Planes, *Phys. Rev. B* **73**, 174413 (2006).
- <sup>16</sup>X. Moya, L. Mañosa, A. Planes, S. Aksoy, M. Acet, E. F. Wassermann, and T. Krenke, *Phys. Rev. B* **75**, 184412 (2007).
- <sup>17</sup>Z. D. Han, D. H. Wang, C. L. Zhang, S. L. Tang, B. X. Gu, and Y. W. Du, *Appl. Phys. Lett.* **89**, 182507 (2006).
- <sup>18</sup>P. A. Bhobe, K. R. Priolkar, and A. K. Nigam, *Appl. Phys. Lett.* **91**, 242503 (2007).
- <sup>19</sup>J. L. S. Llamazares, H. Flores-Zúñiga, D. Ríos-Jara, C. F. Sánchez-Valdes, T. García-Fernández, C. A. Ross, and C. García, *J. Appl. Phys.* **113**, 17A948 (2013).
- <sup>20</sup>M. Acet, *Nat. Mater.* **8**, 854 (2009).
- <sup>21</sup>R. Niemann, O. Heczko, L. Schultz, and S. Fähler, *Appl. Phys. Lett.* **97**, 222507 (2010).
- <sup>22</sup>J. Feuchtwanger, M. L. Richard, Y. J. Tang, A. E. Berkowitz, R. C. O'Handley, and S. M. Allen, *J. Appl. Phys.* **97**, 10M319 (2005).
- <sup>23</sup>J. Liu, N. Scheerbaum, S. Kauffmann-Weiss, and O. Gutfleisch, *Adv. Eng. Mater.* **14**, 653 (2012).
- <sup>24</sup>M. Schmitt, A. Backen, S. Fähler, and M. Kohl, *Microelectron. Eng.* **98**, 536 (2012).
- <sup>25</sup>M. Kohl, D. Brugger, M. Ohtsuka, and T. Takagi, *Sens. Actuators, A* **114**, 445 (2004). Selected papers from Transducers 03.
- <sup>26</sup>C. Biffi and A. Tuiissi, *Opt. Laser. Technol.* **78**, Part B, 42 (2016).
- <sup>27</sup>S. V. Kumar, R. Singh, M. M. Raja, A. Kumar, S. Bysakh, and M. Mahendran, *Intermetallics* **71**, 57 (2016).
- <sup>28</sup>K. V. Peruman, S. Vinodh Kumar, K. Pushpanathan, and M. Mahendran, *Funct. Mater. Lett.* **04**, 415 (2011).
- <sup>29</sup>J. Ortín and A. Planes, *Acta Metall.* **36**, 1873 (1988).
- <sup>30</sup>A. Roytburd, T. Kim, Q. Su, J. Slutsker, and M. Wuttig, *Acta Mater.* **46**, 5095 (1998).
- <sup>31</sup>V. Sánchez-Alarcos, V. Recarte, J. Pérez-Landazábal, S. Larumbe, R. Caballero-Flores, I. Unzueta, J. García, F. Plazaola, and J. Rodríguez-Velamazán, *J. Alloys Compd.* **689**, 983 (2016).
- <sup>32</sup>A. A. Prasanna and S. Ram, *Sci. Tech. Adv. Mater.* **14**, 015004 (2013).
- <sup>33</sup>H. Schermgell and A. Kneissl, *Acta Mater.* **50**, 327 (2002).
- <sup>34</sup>G. Rao, J. Wang, E. Han, and W. Ke, *Mater. Lett.* **60**, 779 (2006).
- <sup>35</sup>A. Ghotbi Varzaneh, P. Kameli, V. R. Zahedi, F. Karimzadeh, and H. Salamat, *Met. Mater. Int.* **21**, 758 (2015).
- <sup>36</sup>A. L. Alves, E. C. Passamani, V. P. Nascimento, A. Y. Takeuchi, and C. Larica, *J. Phys. D.: Appl. Phys.* **43**, 345001 (2010).
- <sup>37</sup>G. D. Liu, X. F. Dai, H. Z. Luo, H. Y. Liu, F. B. Meng, Y. Li, X. Yu, J. L. Chen, and G. H. Wu, *J. Phys. D.: Appl. Phys.* **44**, 045002 (2011).
- <sup>38</sup>A. Ghosh and K. Mandal, *Appl. Phys. Lett.* **104**, 031905 (2014).
- <sup>39</sup>V. Sánchez-Alarcos, J. Pérez-Landazábal, V. Recarte, I. Lucia, J. Vèlez, and J. Rodríguez-Velamazán, *Acta Mater.* **61**, 4676 (2013).
- <sup>40</sup>E. C. Passamani, C. Córdova, A. L. Alves, P. S. Moscon, C. Larica, A. Y. Takeuchi, and A. Biondo, *J. Phys. D.: Appl. Phys.* **42**, 215006 (2009).
- <sup>41</sup>R. Y. Umetsu, R. Kainuma, Y. Amako, Y. Taniguchi, T. Kanomata, K. Fukushima, A. Fujita, K. Oikawa, and K. Ishida, *Appl. Phys. Lett.* **93**, 042509 (2008).
- <sup>42</sup>R. Y. Umetsu, K. Sano, K. Fukushima, T. Kanomata, Y. Taniguchi, Y. Amako, and R. Kainuma, *Metals* **3**, 225 (2013).
- <sup>43</sup>E. Passamani, V. Nascimento, C. Larica, A. Takeuchi, A. Alves, J. Proveti, M. Pereira, and J. Fabris, *J. Alloys Compd.* **509**, 7826 (2011).
- <sup>44</sup>J. Rodríguez-Carvajal, *Physica B* **192**, 55 (1993).
- <sup>45</sup>V. V. Sokolovskiy, V. D. Buchelnikov, M. A. Zagrebina, P. Entel, S. Sahoo, and M. Ogura, *Phys. Rev. B* **86**, 134418 (2012).
- <sup>46</sup>T. Krenke, M. Acet, E. F. Wassermann, X. Moya, L. Mañosa, and A. Planes, *Phys. Rev. B* **72**, 014412 (2005).
- <sup>47</sup>O. C. Kistner and A. W. Sunyar, *Phys. Rev. Lett.* **4**, 412 (1960).
- <sup>48</sup>F. J. B. Dominic and P. E. Dickson, *Mössbauer Spectroscopy* (Cambridge University press, Berlin, 1986).
- <sup>49</sup>J. Schaf, K. L. Dang, P. Veillet, and I. A. Campbell, *J. Phys. F: Met. Phys.* **13**, 1311 (1983).
- <sup>50</sup>H. Y. H. W. H. S. Takeshi Shinohara, K. Sasaki, and T. Okada, *J. Phys. Soc. Jpn.* **50**, 2904 (1981).
- <sup>51</sup>K. Ikeda and S. Takahashi, *Phys. Rev. B* **30**, 3808 (1984).
- <sup>52</sup>S. Takahashi and T. Shinohara, *J. Phys. F: Met. Phys.* **12**, 3115 (1982).
- <sup>53</sup>A. P. Young and J. P. Jakubovics, *J. Phys. F: Met. Phys.* **5**, 1866 (1975).
- <sup>54</sup>T. Kamiyama, T. Shinohara, S. Tomiyoshi, Y. Minonishi, H. Yamamoto, H. Asano, and N. Watanabe, *J. Appl. Phys.* **68**, 4741 (1990).
- <sup>55</sup>D. Merida, J. A. García, V. Sánchez-Alarcos, J. I. Pérez-Landazábal, V. Recarte, and F. Plazaola, *Appl. Phys. Lett.* **104**, 231905 (2014).
- <sup>56</sup>P. K. Michael Kalvius, *The Rudolf Mössbauer Story* (Springer-Verlag Berlin Heidelberg, 2012).
- <sup>57</sup>V. Sánchez-Alarcos, V. Recarte, J. Pérez-Landazábal, C. Gómez-Polo, and J. Rodríguez-Velamazán, *Acta Mater.* **60**, 459 (2012).